Effects of alloying and strain on the magnetic properties of $Fe_{16}N_2$

Liqin Ke,[1] Kirill D. Belashchenko,[2] Mark van Schilfgaarde,[3] Takao Kotani,[4] and Vladimir P. Antropov[1]
[1]*Ames Laboratory US Department of Energy, Ames, Iowa 50011, USA*
[2]*Department of Physics and Astronomy and Nebraska Center for Materials and Nanoscience, University of Nebraska-Lincoln, Lincoln, Nebraska 68588, USA*
[3]*Department of Physics, King's College London, Strand, London WC2R 2LS, United Kingdom*
[4]*Department of Applied Mathematics and Physics, Tottori University, Tottori 680-8551, Japan*
(Received 9 April 2013; published 8 July 2013)

The electronic structure and magnetic properties of pure and doped $Fe_{16}N_2$ systems have been studied in the local-density (LDA) and quasiparticle self-consistent *GW* approximations. The *GW* magnetic moment of pure $Fe_{16}N_2$ is somewhat larger compared to LDA but not anomalously large. The effects of doping on magnetic moment and exchange coupling were analyzed using the coherent potential approximation. Our lowest estimate of the Curie temperature in pure $Fe_{16}N_2$ is significantly higher than the measured value, which we mainly attribute to the quality of available samples and the interpretation of experimental results. We found that different Fe sites contribute very differently to the magnetocrystalline anisotropy energy (MAE), which offers a way to increase the MAE by small site-specific doping of Co or Ti for Fe. The MAE also increases under tetragonal strain.

DOI: 10.1103/PhysRevB.88.024404 PACS number(s): 75.50.Ww, 75.50.Bb, 71.20.Be, 75.30.Cr

I. INTRODUCTION

Ordered nitrogen martensite α''-$Fe_{16}N_2$ was first synthesized in bulk form by quenching of the cubic nitrogen austenite γ-FeN with a subsequent annealing.[1] Quenching initially produces disordered α'-FeN, which then orders during low-temperature annealing to produce α''-$Fe_{16}N_2$. The latter is a metastable phase with a distorted body-centered tetragonal structure, which decomposes into α-Fe and Fe_4N near 500 K.

Interest in α''-$Fe_{16}N_2$ was revived much later when it was synthesized in thin film form and a very large value ($\sim 3\mu_B$) for the average Fe magnetic moment was reported.[2] This result was not independently confirmed until twenty years later.[3] Owing to the rapid development of the magnetic recording technologies, this confirmation inspired numerous studies of thin-film samples. However, the existence of the "giant" Fe moment remains controversial as many researchers did not reproduce these findings, while others confirmed them.[4–6] The lack of consistent and reproducible experimental results may be attributed to the difficulties associated with the preparation of single-crystal $Fe_{16}N_2$ and stabilization of nitrogen, as well as with the accurate measurement of the magnetization in multiphase Fe nitride samples. This issue has recently attracted additional interest due to the search for new permanent magnetic materials without rare-earth elements.[7] A new way to prepare single-phase $Fe_{16}N_2$ powder was recently reported, along with evidence of high maximum energy product ($BH_{\max}$).[8]

Most theoretical studies of the magnetization of α''-$Fe_{16}N_2$ were performed using the local density approximation, generalized gradient approximation (GGA), or LDA + U, though recently Sims *et al.*[9] applied a hybrid functional and the *GW* approximation to this material. In LDA or GGA the magnetic moment of $Fe_{16}N_2$ is only slightly enhanced compared to elemental Fe. Lai *et al.*[10] included electronic correlations within LDA + U and found an enhanced magnetization $M = 2.85\mu_B$/Fe. Wang *et al.*[11–13] identified a localized Fe state coexisting with the itinerant states in x-ray magnetic circular dichroism (XMCD) measurements. They introduced a specific charge transfer between different Fe sites and obtained a large M in LDA + U. However, the choice of the correlated orbitals and the associated value of the Hubbard U parameter is not well defined for metallic systems. For example, the on-site interaction parameters obtained by Sims *et al.*[9] using the constrained random phase approximation (RPA) differ substantially from those proposed by Wang *et al.* The quasiparticle self-consistent *GW* approximation (QS*GW*)[14,15] is more reliable and provides a more satisfactory way to determine the ground state density and magnetic moment. In the present paper we apply this method to $Fe_{16}N_2$.

Studies of exchange interaction, Curie temperature (T_C), and MAE of $Fe_{16}N_2$ met with additional difficulties. In particular, measurements of T_C are hampered by the decomposition of the metastable $Fe_{16}N_2$ into Fe_4N and Fe, which was reported to occur above 200 °C,[6] in the 230–300 °C range,[2] or at 400 °C.[3] Sugita *et al.* extrapolated their data to estimate T_C at 540 °C.[3] Thermal stability of $Fe_{16}N_2$ was reported to increase with addition of Co and Ti[16,17] (up to 700 °C in the Ti case). However, no experimental information is presently available about the T_C of Co or Ti-doped $Fe_{16}N_2$, or of any other $Fe_{16}N_2$ samples stabilized at high temperatures. To the best of our knowledge, there have been no theoretical studies of the exchange interaction and Curie temperature in $Fe_{16}N_2$. Systematic studies of the effects of doping on M and T_C in $Fe_{16}N_2$ also appear to be lacking.

As for the MAE, only a few experimental values were reported, and they are varied and inconclusive. For example, Sugita *et al.*[3] obtained an in-plane MAE, while Takahashi[18] found a large uniaxial MAE. The only available theoretical calculations of MAE used an empirical tight binding (TB) approximation.[19] In this paper we study the magnetization, Curie temperature, and magnetocrystalline anisotropy energy of pure and doped $Fe_{16}N_2$ using several well-tested electronic structure techniques and suggest possible routes for improving its properties for permanent magnet applications.

II. COMPUTATIONAL METHODS

Most LDA, GGA, and QSGW calculations were performed using a full-potential generalization[20] of the standard linear muffin-tin orbital (LMTO) basis set.[21] This scheme employs generalized Hankel functions as the envelope functions. Calculations of MAE were also performed using the recently-developed mixed-basis full-potential method,[22] which employs a combination of augmented plane waves and generalized muffin-tin orbitals to represent the wave functions. The results of a traditional non-self-consistent application of the GW approximation depend on the noninteracting Hamiltonian generating the self-energy. This issue can be particularly problematic for metals. In contrast, the QSGW method does not suffer from this limitation: It is more reliable than the standard GW. This method gives quasiparticle energies, spin moments, dielectric functions, and a host of other properties in good agreement with experiments for a wide range of materials, including correlated ones such as NiO. The details of QSGW implementation[14,15] and applications can be found elsewhere.

The pair exchange parameters were obtained using two linear response approaches:

(i) Static linear-response approach[23] implemented within the atomic sphere approximation (ASA) to the Green's function (GF) LMTO method.[24] In addition to making a spherical approximation for the potential, this method makes the long-wave approximation (LWA), so that the pair exchange parameter is proportional to the corresponding spin susceptibility χ_{ij}.[25] The exchange parameters A_{ij} obtained in this method are related to the parameters of the classical Heisenberg model

$$H = -\sum_{ij} J_{ij}\mathbf{S}_i \cdot \mathbf{S}_j, \tag{1}$$

by the following renormalization for ferromagnetic(FM) and antiferromagnetic(AFM) cases:

$$\begin{aligned} J_{ij} &= A_{ij}/\mathbf{S}_i\mathbf{S}_j \\ &= 4A_{ij}/\mathbf{m}_i\mathbf{m}_j = \begin{cases} 4A_{ij}/m_i m_j & \text{FM} \\ -4A_{ij}/m_i m_j & \text{AFM} \end{cases} \end{aligned} \tag{2}$$

where $\mathbf{m}_i$ is the magnetic moment on site i. With this renormalization all results obtained for the Heisenberg model Eq. (1) can be used directly. Thus, parameters A_{ij} always stabilize (destabilize) the given magnetic configuration and can be treated as stability parameters. Curie temperature in the spin classical mean field approximation (MFA) is simply $T_C = 2/3\sum_{ij} A_{ij}$.

(ii) Dynamical linear response approach with the bare susceptibility $\chi(\mathbf{q},\omega)$ calculated in the full product basis set representation using the LDA or QSGW electronic structure.[26] The results are then projected onto the functions representing local spin densities on each magnetic site, which gives a matrix $\chi_{ij}(\mathbf{q},\omega)$ in basis site indices.[26] This projection corresponds to the rigid spin approximation. The inversion of this matrix with a subsequent Fourier transform provides the real-space representation of the inverse susceptibility representing the effective pair exchange parameters:

$$J_{ij} = \lim_{\omega\longrightarrow 0}\frac{1}{\Omega_{BZ}}\int d\mathbf{q}\,[\chi(\mathbf{q},\omega)]^{-1}\,e^{i\mathbf{q}\mathbf{R}_{ij}}. \tag{3}$$

T_C is calculated both in the MFA[27] and the RPA-Tiablikov[28] approximations. The actual T_C may usually be expected to lie between the results of these two approximations.

To address the effects of doping, we used our implementation of the coherent potential approximation (CPA) within the TB-LMTO code, which follows the formulation of Turek *et al.*[29] and Kudrnovský *et al.*[30] A coherent interactor matrix Ω_i is introduced for each basis site i treated within CPA. At self-consistency $g_{ii} = (\mathcal{P}_i - \Omega_i)^{-1}$, where $\mathcal{P}_i$ is the coherent potential matrix for site i, and g_{ii} is the on-site block of the average auxiliary LMTO GF matrix $g = (\mathcal{P} - S)^{-1}$. This on-site block is extracted from the Brillouin zone integral of $g(\mathbf{k})$. The conditionally averaged GF at site i occupied by component a is $g^a_{ii} = (P_a - \Omega)^{-1}$, and the CPA self-consistency condition can be written as $g_{ii} = \sum_a c^a_i g^a_{ii}$; here c^a_i is the concentration of component a at site i. Using this equation, at the beginning of each iteration the stored matrices Ω_i are used to obtain an initial approximation to $\mathcal{P}_i$. In turn, $\mathcal{P}_i$ is used in the calculation of g_{ii} by a Brillouin zone integral. The next approximation for Ω_i is obtained from $\Omega_i = \mathcal{P}_i - g^{-1}_{ii}$. These output matrices are then linearly mixed with the input Ω_i matrices at the end of the iteration.

We found that the mixing coefficient of 0.4 for Ω_i works well in most cases. For fastest overall convergence, we found that it is usually desirable to iterate CPA iterations until the Ω_i matrices are converged to a small tolerance, and only then perform the charge iteration. The convergence of Ω is done separately for each point on the complex contour to the same tolerance. With this procedure, fairly aggressive Broyden mixing can be used for LMTO charge moments. CPA convergence at each charge iteration usually takes 10–50 iterations depending on the imaginary part of the energy and the selected tolerance. At the beginning of the calculation, the Ω_i matrices are set to zero; afterwards they are stored and reused for subsequent iterations. In order to avoid unphysical symmetry-breaking CPA solutions (which otherwise often appear), the coherent potentials and the $\mathbf{k}$-integrated average auxiliary GF are explicitly symmetrized using the full space group of the crystal. As a result, the use of CPA does not impose any restrictions on the symmetry of the crystal. Calculations reported here were performed without using charge screening corrections for the Madelung potentials and total energy.

The effective exchange coupling in CPA is calculated as

$$A_0(c) = cA_X(c) + (1-c)A_Y(c), \tag{4}$$

where the component-specific $A_i(c)$ are obtained using the conditionally averaged GF and the formalism of Ref. 31.

For MAE calculations the self-consistent solutions are found including spin-orbit coupling (SOC) terms of order $1/c^2$. The MAE is defined below as $K = E_{100} - E_{001}$, where E_{001} and E_{100} are the total energies for the magnetization oriented along the [001] and [100] directions, respectively. Positive (negative) K corresponds to uniaxial (planar) anisotropy. We used a $24\times24\times24$ k-point mesh for MAE calculations to ensure sufficient convergence; MAE changed by less than 2% when a denser $32\times32\times32$ mesh was employed. All calculations

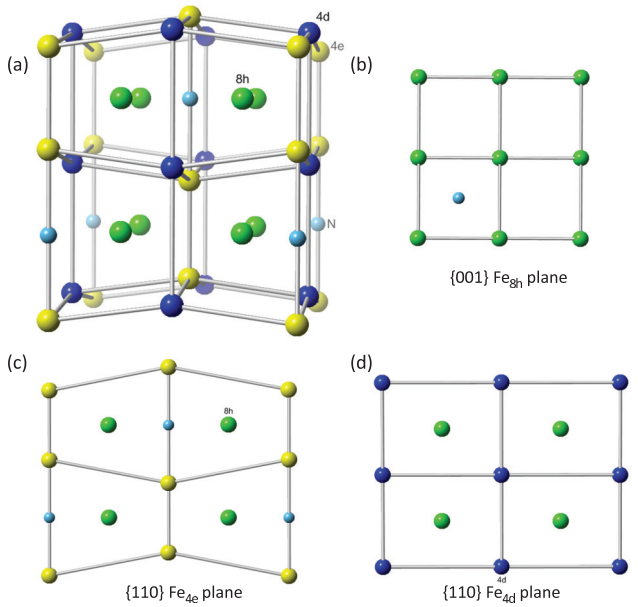

FIG. 1. (Color online) (a) Crystal structure of $Fe_{16}N_2$. The experimental atomic positions are shown. Relaxed structure has slightly different z_{4e} and x_{8h}. (b) {001} plane with 8*h* and N atoms. (c) {110} plane with 4*e*, 8*h*, and N atoms. (d) {110} plane with 4*d* and 8*h* atoms.

except QSGW were performed with both LDA[32] and GGA[33] exchange-correlation potentials for comparison.

III. RESULTS AND DISCUSSION

The crystal structure of $Fe_{16}N_2$ is body-center-tetragonal (bct) with space group $I_{4/mmm}$(#139). It may be viewed as a distorted $2 \times 2 \times 2$ bct-Fe superlattice with $c/a = 1.1$. Crystal structure of $Fe_{16}N_2$ was first identified by Jack.[1] Here we use lattice constants $a = b = 5.72$ Å $c = 6.29$ Å and atomic position parameters $z_{4e} = 0.3125$ and $x_{8h} = 0.25$ from Jack's work as the experimental structure (see Fig. 1).

We also relaxed the structure by minimizing the total energy in LDA and obtained $z_{4e} = 0.293$ and $x_{8h} = 0.242$, nearly identical to that obtained by Sawada *et al.*[34] The primitive cell contains one N and eight Fe atoms divided into three groups indicated by Wyckoff sites: two 4*e*, four 8*h*, and two 4*d* sites (correspondingly first, second, and third neighbors to N).

A. Magnetic moments and electronic structure

Table I shows the atomic spin moment m_i at the three Fe sites and magnetization M (orbital magnetic moment is small, hereafter we only include spin magnetization in M). Within the LDA, $M = 2.38\mu_B$/Fe was obtained, in good agreement with previously reported calculations.[4–6] The enhancement relative to elemental bcc-Fe has been attributed to the size effect.[35] QSGW gives $M = 2.59\mu_B$/Fe, about 9% larger than LDA. While it is known that GW enhances spin moments relative to LDA, to ensure the genuineness of this enhancement of moment, we also carried out the QSGW calculation of bcc-Fe and found that QSGW enhance the LDA magnetic moment in elemental Fe by only ~2% (2.20→2.24μ_B).

TABLE I. Atomic spin magnetic moment m_i and spin magnetization M in $Fe_{16}N_2$ in different methods. Calculations are in the LDA unless GGA or QSGW is specified.

	$m_i(\mu_B)$[a]				m[b]	M[c]	
Method	4*e*	8*h*	4*d*	N	(μ_B)	(μ_B/Fe)	(emu/g)
ASA	2.07	2.40	3.03	−0.06	2.48	2.47	239
ASA-GF	2.10	2.41	2.99	−0.10	2.48	2.47	239
FP	2.08	2.32	2.84	−0.05	2.39	2.38	231
FP(GGA)	2.21	2.40	2.86	−0.04	2.47	2.43	236
QSGW	2.24	2.55	3.12	−0.01	2.62	2.59	251

[a]Spin moment inside atomic or muffin-tin sphere.
[b]Average of the atomic spin moments of all Fe sites without taking account of interstitial and N sites.
[c]Average spin moments within the cell (with taking account of interstitial and N sites).

Sims *et al.*[9] found a similar M in their GW calculation while they also obtained a larger magnetization enhancement in bcc-Fe with $M = 2.65\mu_B$/Fe. Considering $Fe_{16}N_2$ consists of about 87% Fe, the 9% enhancement we find nontrivial. However, it is still well below $M = 2.85\mu_B$/Fe, obtained in LDA + U by Lai *et al.*[10] The spin moment on the 4*d* site reaches $m_i = 3.11\mu_B$ in QSGW, though we do not observe any obvious charge transfer from 4*d* to 4*e* and 8*h* sites in QSGW, relative to the LDA. Hence, we can not attribute the enhancement of M to the charge transfer as suggested by others[11–13].

Density of states (DOS) calculated within LDA and QSGW are shown in Fig. 2. The LDA result is similar to previously reported results. A careful examination of the band structure reveals that QSGW significantly modifies the energy bands near E_F, relative to LDA. It has a slightly larger on-site exchange, widening the split between the majority and minority DOS and increasing M by about 9%. Both DOS figures show hybridization between N-2*p* and Fe-3*d* states at around −7 eV, indicating that QSGW does not strongly modify the relative alignment of N-2*p* and Fe-3*d* levels. Comparing the partial DOS reveals that bands are slightly wider and hybridization is overestimated in LDA, as is typical since LDA tends to overestimate 3*d* bandwidths slightly. The DOS also show hybridization is stronger in the 4*e* and 8*h* channels while weaker in the 4*d* channels, which are the furthest removed from N. Also, as typical with second row elements, QSGW pushes the N-2*s* bands down relative to LDA, from −16.2 eV to −18 eV. The N-2*s* also hybridizes with Fe-4*e* and Fe-8*h*. However there is almost no hybridization with the furthest Fe-4*d* at all because the N-2*s* orbitals are very localized.

B. Exchange coupling and Curie temperature

The Heisenberg model parameters J_{ij} using LDA-ASA in the LWA, FP-LDA, and FP-QSGW are plotted in Fig. 3 and tabulated in Table II. The two LDA results are quite similar, confirming that the ASA and the LWA form a reasonable approximation. QSGW shows some differences, particularly reducing those interactions which are AFM.

The structure of J_{ij} is much more complicated in $Fe_{16}N_2$ than in elemental bcc-Fe. The vectors connecting the nearest 8*h*–4*e* or 8*h*–4*d* sites are nearly along the [111] direction;

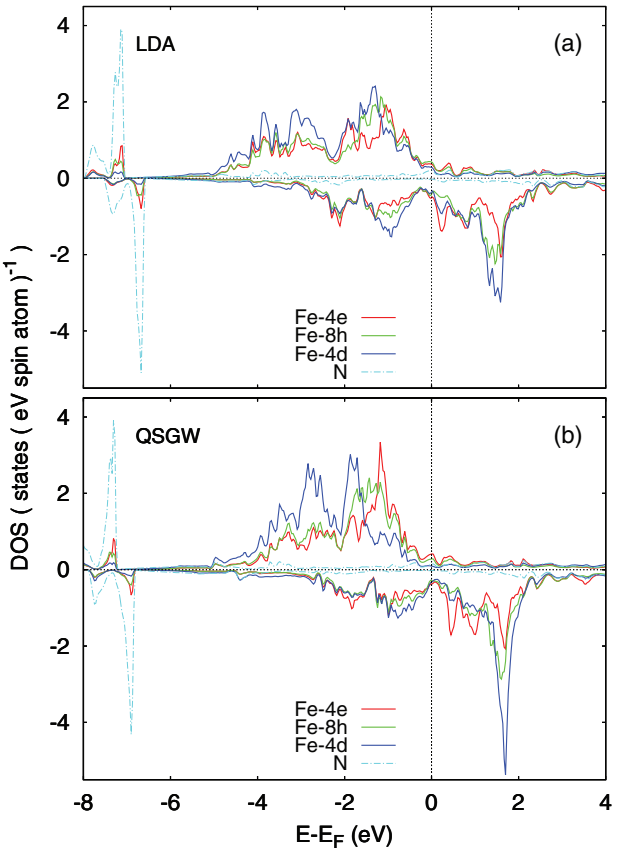

FIG. 2. (Color online) Site and spin-projected densities of states within LDA (a) and QSGW (b).

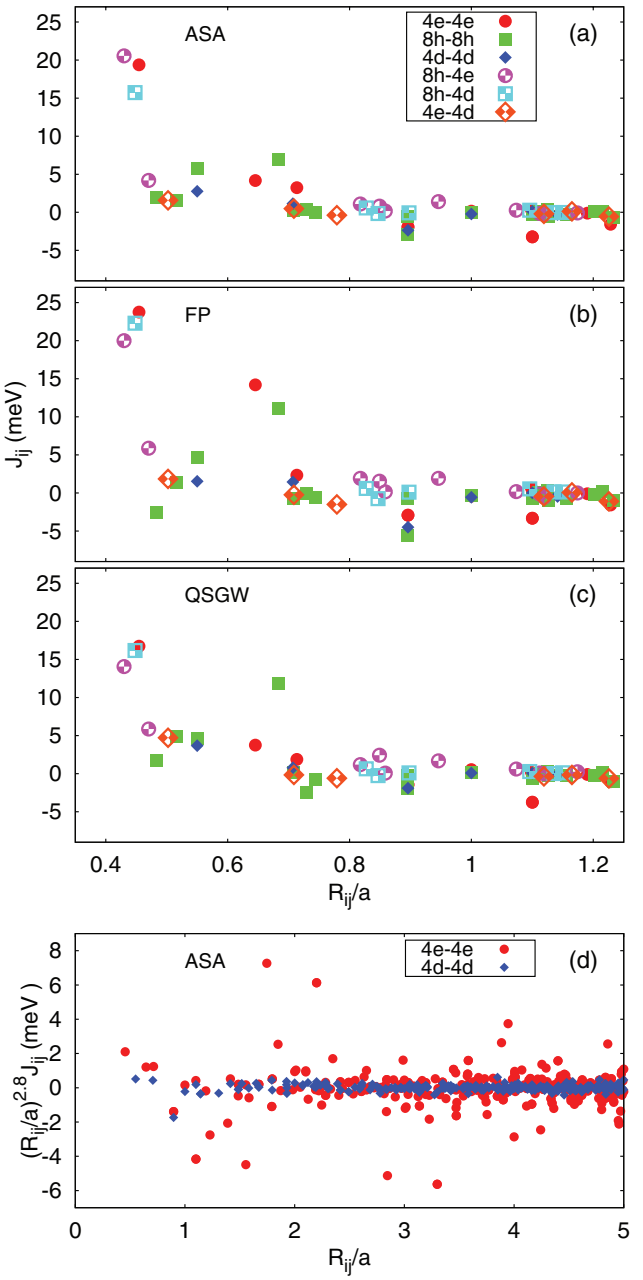

FIG. 3. (Color online) Real-space magnetic exchange parameters J_{ij} in $Fe_{16}N_2$ within ASA-GF (a), FP (b), and QSGW (c) as functions of distance R_{ij}/a. (d) $(R_{ij}/a)^{2.8}J_{ij}$ in ASA-GF as a function of distance R_{ij}/a. The in-plane lattice constant a in $Fe_{16}N_2$ is twice as large as in bcc-Fe.

the magnetic interactions between them are generally large. In comparison, the largest interaction is also between the nearest sites connected by vectors along the [111] direction in bcc-Fe. J_{ij} between $8h$–$4e$ sites is very anisotropic due to the distortion of the lattice around N atom. Similar anisotropy was also found for the in-plane couplings on the $8h$ lattice. Interestingly, a large coupling ($J_{ij} = 23.75$ meV in the FP-LDA calculation) occurs between two $4e$ atoms along [001]. This pair has been squeezed together by neighboring N atoms. Since exchange coupling is sensitive to the distance between those two sites, we also examined this exchange parameter for the experimental atom coordinates, for which the bond length of the $4e$–$4e$ pair shrinks from 2.60 to 2.36 Å, and found that this J_{ij} increases from 23.75 to 36.55 meV, indicating significant exchange-striction effect. The second nearest $4e$–$4e$ coupling (two Fe atoms with a N atom between them along the $\langle 110 \rangle$ direction) is 14.2 meV in FP and 4.18 meV in ASA. The relatively large disagreement may be a consequence of the shape approximation used in ASA, considering the presence of N atom and strong lattice distortion around this pair of atoms.

The calculated magnetic interactions between different types of atoms have very different spatial dependence and correspondent asymptotic behavior. To demonstrate it explicitly on Fig. 3(d) we show J_{ij} scaled with $(R_{ij}/a)^{2.8}$. With this renormalization J_{ij} between atoms on 4e positions (smaller moments) are approximately constant in this range of distances (long-ranged interaction), while J_{ij} between Fe atoms on 4d sites (with the largest moments) decay much faster (short-ranged interaction), corresponding to more localized moment behavior. Such very different asymptotic behavior suggests that these localized and delocalized interactions correspond to Fermi surface shapes with different dimensionalities.

T_C is calculated from the exchange parameters and tabulated in Table II. RPA values are about 30% smaller than the MFA ones. Typically experimental values fall between the MFA and RPA results, with the RPA being closer to the experiment in normal three dimensional systems. In the present case, however, the reported extrapolated experimental estimate

TABLE II. Pairwise exchange parameters of the Heisenberg model J_{ij}(meV) and T_C(K) calculated with different methods.

	$\|R_{ij}\|/a$	direction			ASA	FP	*GW*
4*e*–4*e*	0.454	0	0	−0.455	19.37	23.75	16.75
	0.645	0	0	0.645	4.18	14.20	3.76
	0.713	−0.5	−0.5	0.095	3.24	2.33	1.88
	0.895	−0.5	−0.5	−0.550	−1.92	−2.91	−1.44
8*h*–8*h*	0.483	0	−0.484	0	2.00	−2.55	1.69
	0.516	0	0.516	0	1.49	1.37	4.84
	0.550	0.016	0.016	0.550	5.74	4.60	4.67
	0.684	−0.484	−0.484	0	7.00	11.07	11.80
	0.707	0.516	−0.484	0	0.20	−0.68	0.13
	0.730	0.516	0.516	0	0.39	−0.01	−2.50
4*d*–4*d*	0.550	0	0	0.550	2.76	1.54	3.67
	0.707	−0.5	0.5	0	1.15	1.44	0.78
	0.895	−0.5	−0.5	0.550	−2.37	−4.49	−1.90
4*e*–8*h*	0.430	−0.258	−0.258	−0.227	20.55	20.00	14.08
	0.470	0.242	0.242	0.323	4.20	5.88	5.88
8*h*–4*d*	0.448	0.258	−0.242	0.275	15.73	22.30	16.18
	0.827	−0.242	−0.742	−0.275	0.58	0.60	0.64
4*d*–4*e*	0.502	−0.5	0	0.048	1.56	1.85	4.72
	0.708	0	−0.5	−0.502	0.49	−0.23	−0.16
	T_C(MFA)				1552	1621	1840
	T_C(RPA)				1118	1065	1374

$T_C = 810$ K[3] is smaller than both the MFA and RPA values, and smaller than the one in bcc-Fe.[24] This is rather unusual. In bcc-Fe, we estimate T_C to be ∼1300 K and ∼900 K in the MFA and RPA, respectively, which bracket the experimental value of 1023 K (as is typical). Contrary to experiment, our calculated T_C for $Fe_{16}N_2$ is *higher* than for bcc Fe in all our estimations. Such disagreement between theory and experiment is much larger in $Fe_{16}N_2$ than other Fe-rich phases. The disagreement may originate from approximations to the theory (absence of spin quantum effects, temperature dependence of exchange, among others) that uniquely affect $Fe_{16}N_2$, or alternatively from the experimental interpretation of the measured T_C. We cannot completely discount the former possibility, but for this local-moment system, it is unlikely that the most serious errors originate in density functional theory that generate exchange parameters. For instance, parameters generated from QS*GW* also do not improve agreement with the experiment; indeed this increases the discrepancy. On the other hand, as noted in the introduction $Fe_{16}N_2$ decomposes with increasing T; moreover, there is a transition to the (nonmagnetic) γ phase at 1185 K. Since the measured $M(T)$ is not a measurement of the single-phase material, it is still unknown what is the experimental value for the T_C in a single-phase $Fe_{16}N_2$. Unfortunately, disentangling the structural and magnetic degrees of freedom is very difficult, experimentally. Finally, if M increases in $Fe_{16}N_2$, as is observed and predicted, T_C should increase. Thus we conclude that T_C in high quality samples of pure $Fe_{16}N_2$ is probably larger than what has been reported so far, and larger than in pure bcc-Fe.

Let us now discuss the influence on T_C when other atoms substitute for Fe or N. The CPA is an elegant, single-site *ab initio* approach to study substitutional alloys. We have implemented the CPA, including a MFA estimate for T_C, within the ASA. As we have seen by comparing exchange interactions in the ASA to those without this approximation, the ASA does not seem to be a serious approximation to the LDA in this material.

Figure 4 shows the M and and the normalized effective exchange (or MFA estimation of T_C in units of pure $Fe_{16}N_2$)

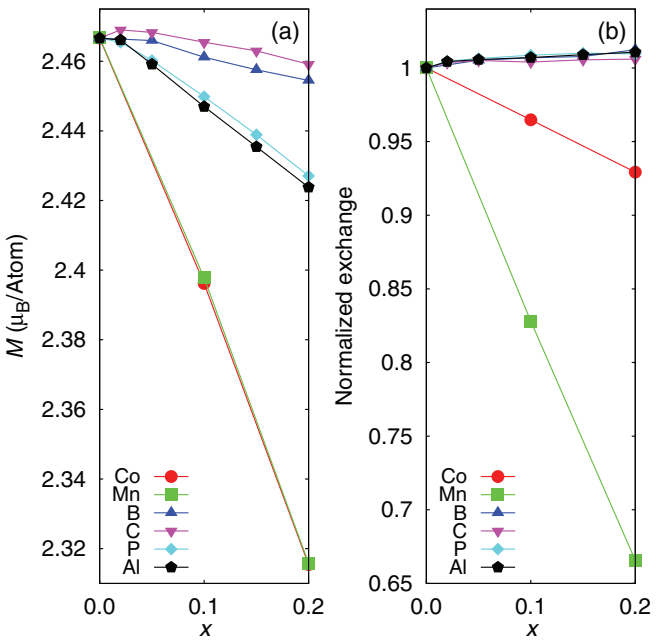

FIG. 4. (Color online) Spin magnetization M (a) and normalized exchange $J_0/J_0(Fe_{16}N_2)$ (with respect to pure $Fe_{16}N_2$) (b) as functions of doping concentration in $Fe_{16}N_2$. The concentration x of doping element T is defined as $(Fe_{1-x}T_x)_{16}N_2$ with Fe site doping (T = Co,Mn); and $Fe_{16}(N_{1-x}T_x)_2$ with N site doping(T = B, C, P, and Al) .

TABLE III. Component-resolved atomic spin moments m_i (the atomic spin moment of substitutional component are given in parentheses), magnetization M, and exchanges J_0 in Co- and Mn-doped $Fe_{16}N_2$ calculated within ASA-GF.

		$m_i(\mu_B)$							J_0(meV)					
Substituent	x	4e		8h		4d		$M(\mu_B$/atom)	4e		8h		4d	
Co	0.00	2.10	(1.44)	2.41	(1.68)	2.99	(2.11)	2.47	12.95	(11.37)	15.70	(14.62)	16.96	(19.42)
	0.10	2.09	(1.34)	2.43	(1.64)	3.01	(2.09)	2.40	11.97	(9.62)	15.45	(13.56)	16.70	(18.68)
	0.20	2.08	(1.27)	2.45	(1.62)	3.02	(2.08)	2.32	11.24	(8.47)	15.19	(12.91)	16.50	(18.07)
Mn	0.00	2.10	(1.88)	2.41	(2.25)	2.99	(3.23)	2.47	12.96	(7.05)	15.70	(6.57)	16.97	(1.07)
	0.10	2.07	(1.75)	2.35	(2.04)	2.96	(3.03)	2.40	12.03	(5.64)	14.01	(4.03)	14.97	(−1.10)
	0.20	2.06	(1.64)	2.30	(1.85)	2.93	(2.90)	2.32	11.15	(4.41)	12.59	(2.09)	13.22	(−2.69)

with doping by different elements. Both Co and Mn doping cause T_C to decrease. On the other hand, with N site being doped with B, C, P, or Al elements, T_C and M change slightly and the Fermi surface character is barely affected.

As shown in Fig. 4, Co or Mn-doped $Fe_{16}N_2$ decrease moment and exchange coupling. We neglected the possible site preference effect in this calculation, and doped all three Fe sites with equal probability. Table III shows the magnetic moment and J_0 parameters of Fe and substitutional components on all three different Fe sites. It indicates an opportunity to increase T_C by using a separate Co doping on Fe-4d sites.

Magnetic moments of the Fe component decrease with Mn doping and slightly increase with Co doping. With Co doping, the Fe moments on 8h and 4d sites do slightly increase, however this increment is not big enough to overcome the decrease resulting from Co substituting for Fe—the system behaves more like a localized moments system. We also carried out the FP calculation of Fe_7CoN, with one out of eight Fe atoms being replaced by a Co atom and confirmed that the magnetization decreases, especially when Co replaces the Fe on the 4e site. This is consistent with the CPA results. Mn substituents have larger magnetic moments than Co substituents. However, Mn doping decreases moments on Fe sites. Overall, the dependence of the total magnetic moments on substituent concentration are almost exactly the same with Co and Mn doping. Another interesting observation is that magnetic moments of both substituents decrease with increasing of doping concentration. This can be explained by the partial density of states as shown in Fig. 5. The magnetic moment of Co slightly decreases with increasing of doping concentration. As shown in Fig. 5, the unoccupied DOS peak right above the Fermi energy (E_F) in the minority spin channel moves toward it. More electrons fill in the minority channel and decrease the magnetic moment as doping increases. With Mn doping, on the other hand, the peak in the majority channel right below E_F becomes less pronounced. It shifts toward E_F and decreases the magnetic moment of Mn component. For the Fe component DOS, there is no peak structure near the E_F, and magnetic moment is much less sensitive to the substitutional concentration.

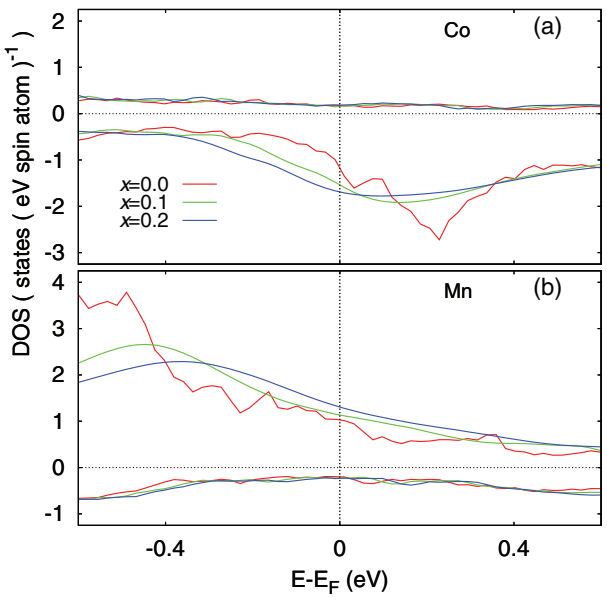

FIG. 5. (Color online) Densities of state of substitutional component in random alloy $(Fe_{1-x}Co_x)_{16}N_2$ (a) and $(Fe_{1-x}Mn_x)_{16}N_2$ (b).

C. Magnetic anisotropy

Values of MAE from previous works are summarized in Table IV. Results of present works are shown in Table V. All calculations are carried out within LDA unless GGA is specified. For the pure $Fe_{16}N_2$, both experimental and optimized structures are investigated. Note that doping and SOC lower the symmetry, and the degeneracy of l varied. Within LDA, a uniaxial magnetic anisotropy $K = 144 \times 10^5$ erg/cm^3 was obtained with experimental atomic coordinates. Structural optimization gives a smaller MAE with $K = 103 \times 10^5$ erg/cm^3. GGA gives smaller MAE than LDA. It is usually nontrivial to analyze the origin or site dependence of magnetic anisotropy. Below we define the atomic magnetic

TABLE IV. Previous works on magnetic anisotropy in $Fe_{16}N_2$.

Method		$K(\frac{10^5 \text{erg}}{\text{cm}^3})$	Easy axis	Ref.
Exp.	Sugita *et al.*	4.8	[100]	3
	Takahashi *et al.*	200[a]	[001]	18
	Takahashi *et al.*	97	[001]	19
	Kita *et al.*	44	[001]	36
	Ji *et al.*	100[b]	[001]	37
TB[c]	Uchida *et al.*	140	[001]	19

[a]Value of $(K_1 + K_2)$.
[b]Measured in partial-ordering $Fe_{16}N_2$; author claimed MAE should be much higher for the single-phase sample.
[c]Tight binding approximation.

TABLE V. The MAE K, on-site orbital magnetic moment l, and the AMAE Δ with different spin quantization axis direction in pure, Co-doped, and Ti-doped $Fe_{16}N_2$. Spin quantization axis direction **e** are along [001], [100], and [110] directions, respectively. With the spin along [100] and [110], Δ and K values (with respect to [001] direction) directions are given. To estimate Δ, $\xi_i = 50{,}70$ meV had been used for Fe and Co atoms, respectively.

		K		$l(10^{-3}\mu_B)$			Δ
	e	$\frac{\mu eV}{Fe}$	$\frac{10^5 erg}{cm^3}$	$4e$	$8h$	$4d$	$\frac{\mu eV}{Fe}$
Exp.[a]	001			54	45	71	
	100	116	144	35	49	64	
	110	116	144	36	58 39	64	
Exp.[a]	001			52	44	68	
GGA	100	105	131	36	48	61	110
	110	105	131	36	57 39	61	110
Theo.[b]	001			62	46	67	
	100	84	103	39	50	63	137
	110	84	103	39	58 41	63	137
Theo.[b]	001			56	43	62	
GGA	100	52	65	38	47	58	
	110	52	65	38	55 40	58	
Fe_7CoN	001			91[d] 72	47	76	
$(4e)$[c]	100	165	206	49[d] 30	49	61 64	337
	110	165	206	49[d] 30	61 36	63	336
	001			63	69[d] 41 41 44	70	
$(8h)$	100	42	52	36	77[d] 46 50 47	67	123
	110	16	20	40	90[d] 38 38 56	67	81
	001			63	51	120[d] 81	
$(4d)$	100	138	171	33 38	52	106[d] 70	271
	110	138	171	36	62 42	106[d] 70	271
Fe_7TiN	001			11[d] 63	40	69	
$(4e)$	100	127	158	10[d] 27	46	65 65	62
	110	127	158	10[d] 27	55 38	65	62
	001			55	14[d] 48 48 41	69	
$(8h)$	100	57	71	38	13[d] 48 50 50	65	122
	110	43	53	35	13[d] 41 41 62	68	83
	001			60	40	14[d] 69	
$(4d)$	100	102	127	38 38	45	13[d] 67	83
	110	103	128	38	52 38	13[d] 67	83

[a]Exp. the experimental crystal structure was used.
[b]Theo. the theoretically optimized crystal structure was used.
[c]Doping site of the substitutional atom.
[d]Orbital magnetic moments of the substitutional atoms.

anisotropy energy (AMAE) Δ_i as half of the difference of the SOC energies along different magnetic field directions, that is in turn defined by the corresponding anisotropy of orbital magnetic moments:

$$\sum \Delta_i(\theta = 90^\circ) = \sum \xi_i m_i \left(l_i^{001} - l_i^{100}\right)/4, \qquad (5)$$

where ξ_i is a SOC parameter, while m_i and l_i are atomic spin and orbital magnetic moments correspondingly. The sum of Δ_i can be compared with the total MAE K obtained using the total energies. This approach takes into account the SOC anisotropy and its renormalization by crystal field effects. We further assume that the spin moment has very weak anisotropy[38] and the main change in $\xi \mathbf{L} \cdot \mathbf{S}$ product comes from the change of orbital magnetic moment (see also Ref. 39). This is the case for $Fe_{16}N_2$ (see Table V). For the pure $Fe_{16}N_2$, when the spin quantization axis rotates from [100] to [001], l decreases on $8h$ sites, but increases on $4d$ and $4e$. While l depends on site, the total l increases during this rotation, which agrees with the predicted uniaxial character of MAE. When the spin quantization axis points along [110], SOC lowers the symmetry, and splits the four equivalent $8h$ sites into two pairs with l increasing on one pair and decreasing on the other.

As shown in Fig. 6, there is a strong correlation between K and Δ (with respect to magnetic field along [001] direction, and atomic value $\xi_i = 50$ meV is used for all three different Fe sites for simplicity), where i indicates all atomic sites. Obviously, the atomic $8h$ sites make negative contributions to the desired uniaxial MAE, while $4e$ and $4d$ sites make positive contributions. Thus, one may hope that doping on $8h$ site, thus eliminating negative (in-plane) contribution to MAE, may improve the uniaxial MAE.

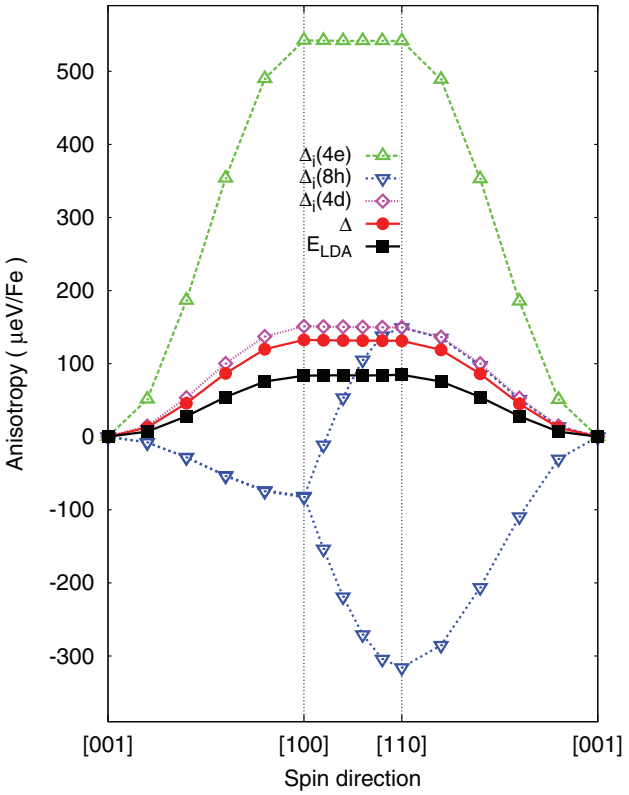

FIG. 6. (Color online) AMAE on $4e$, $8h$, $4d$ Fe sites (Δ_i) and their average value (Δ) and the LDA total energy relative to the ground state (E_{LDA}) as functions of spin quantization axis rotation.

Since Co and Ti doping had been reported to stabilize the $Fe_{16}N_2$ phase,[16,17] it seems logical to study the prediction above using these dopants. We replace one out of eight Fe atoms in the primitive cell with a Co or Ti atom and relax the atomic positions within LDA and then study the anisotropy. If we replace one of four $8h$ atoms with a Co atom, we find that the Co atom has a larger l than any other Fe sites, however, it does not eliminate the negative contribution from $8h$ sites. Instead, it makes K smaller. Also l and then K along the [100] and [110] directions become more anisotropic. Surprisingly, however, with a Co atom on $4e$ or $8h$ sites, the l difference between out-of-plane and in-plane cases becomes even larger on $4e$ and $4d$ sites and smaller on $8h$ sites. In other words, it makes the positive contribution from $4e$ and $4d$ sites stronger and the negative contribution from $8h$ sites smaller. As a result, calculated MAE is doubled ($K = 206\times10^5$ erg/cm^3) within LDA with doped Co being on the $4e$ site. A similar effect had been found with Ti doping. K increases when Ti is substituted on the $4e$ and $4d$ sites and decreases when substituted on $8h$. Unlike the Co doping, magnetic orbital moments of Ti atom are small and barely change with spin rotation. Generally, for the same structure, K is always strongly correlated with Δ. The larger Δ is, the larger K is along that specific spin quantization direction. However, this correlation may no longer hold true with different structures. For example, in Fe_7TiN, Δ is the largest with Ti doped on $8h$ site, however K is much smaller than those with Ti doped on $4e$ and $4d$ sites.

Tetragonality is another factor which may affect the anisotropy in a significant way. Let us compare $Fe_{16}N_2$ with bct-Fe, where even for $c/a = 1.1$ (the c/a ratio for $Fe_{16}N_2$) MAE is still rather tiny.[40] In Fig. 7 the calculated MAE in $Fe_{16}N_2$ is shown as a function of c/a. This dependence is much stronger than in bct-Fe and we assume that MAE mostly originates from distortion of Fe sublattice around the N atom and the Fe-N hybridization. Experimentally, the large tetragonality can be obtained in films, where it can be tuned by the nitrogen concentration.[37] However, according to our results above, doping bulk $Fe_{16}N_2$ in a way that increases c/a may lead to MAE increase. The MAE and AMAE are well correlated as shown in Fig. 7. Within this c/a range, the spin magnetization varies within 2%; it is not likely to be responsible for the MAE increase. On the other hand the anisotropy of orbital moment strongly correlates with MAE and is probably responsible for its enhancement as tetragonality increases. Orbital magnetic moments can be measured more precisely, so new XMCD types of experiments for this system are desirable.

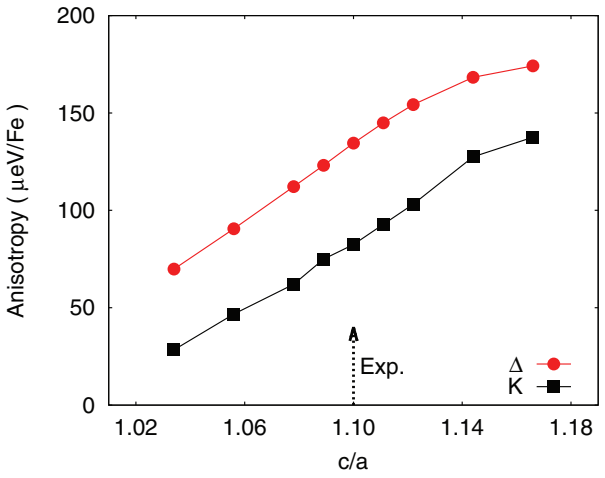

FIG. 7. (Color online) K and the Δ as functions of c/a in $Fe_{16}N_2$. The ideal crystal structure without strain has $c/a = 1.1$. For each c/a, the atomic positions are relaxed with volume being conserved.

IV. CONCLUSION

In this study of intrinsic magnetic properties of $Fe_{16}N_2$, our LDA results for magnetization agree with previously reported values while QSGW increases magnetization by 9%. This enhancement is largely due to on-site exchange splitting between the d minority and majority states—an effect seen in many other magnetic systems such as NiO and MnAs.[26,41] In $Fe_{16}N_2$ in particular, we find no evidence of localized states or correlations not already found in Fe. Taking together all of those factors we expect that the QSGW prediction for M is not far from what should be observed in the ideal $Fe_{16}N_2$ compound. We find no evidence of charge transfer between different Fe sites as proposed elsewhere. Thus, the theoretical magnetization predicted for $Fe_{16}N_2$ does not exceed the maximum on the Slater-Pauling curve ($\sim2.5\mu_B$) and is smaller than the corresponding maximum of magnetization observed in Fe-Co alloys, which may still be considered as a record holder among d atomic magnets.

LDA calculations predict T_C significantly larger than the experimental value; the QSGW result is even larger. We assume that $Fe_{16}N_2$ will have a higher T_C if one can find

a way to stabilize it. Effects of doping by various elements on M and T_C were studied in the LMTO-CPA approximation. Various dopants affect M and T_C differently; but unfortunately no dopants we considered enhanced M or T_C.

A uniaxial magnetocrystalline anisotropy $K = 103 \times 10^5$ erg/cm^3 was calculated in the LDA with the theoretically optimized crystal structure. K is strongly correlated with the atomic magnetic anisotropy energy due to spin-orbit coupling only. We found it can be increased by increasing c/a or by adding a small amount of Co or Ti atoms on 4*e* or 4*d* sites.

$Fe_{16}N_2$ is one of the more promising candidates for permanent magnets that do not contain rare-earth elements. We believe that there is room for improvement and we studied several possible routes to obtain better properties. A further investigation on increasing the thermal stability and/or changing crystal structure tetragonality is desired.

ACKNOWLEDGMENTS

This work was supported by the US Department of Energy, Office of Energy Efficiency and Renewable Energy (EERE), under its Vehicle Technologies Program, through the Ames Laboratory. Ames Laboratory is operated by Iowa State University under contract DE-AC02-07CH11358. K.D.B. acknowledges support from NSF through Grant Nos. DMR-1005642, EPS-1010674 (Nebraska EPSCoR), and DMR-0820521 (Nebraska MRSEC).

[1] K. H. Jack, Proc. R. Soc. A **208**, 200 (1951).
[2] T. K. Kim and M. Takahashi, Appl. Phys. Lett. **20**, 492 (1972).
[3] Y. Sugita, K. Mitsuoka, M. Komuro, H. Hoshiya, Y. Kozono, and M. Hanazono, J. Appl. Phys. **70**, 5977 (1991).
[4] J. M. Cadogan, Aust. J. Phys. **50**, 1093 (1997).
[5] J. M. D. Coey, J. Appl. Phys. **76**, 6632 (1994).
[6] M. Takahashi and H. Shoji, J. Magn. Magn. Mater. **208**, 145 (2000).
[7] J. Coey, Scri. Mater. **67**, 524 (2012).
[8] Conference on Critical Materials for a Clean Energy Future, October 4–5, 2011, Workshops hosted by the US Department of Energy, Washington, DC.
[9] H. Sims, W. H. Butler, M. Richter, K. Koepernik, E. Şaşıoğlu, C. Friedrich, and S. Blügel, Phys. Rev. B **86**, 174422 (2012).
[10] W. Y. Lai, Q. Q. Zheng, and W. Y. Hu, J. Phys.: Condens. Matter **6**, L259 (1994).
[11] J.-P. Wang, N. Ji, X. Liu, Y. Xu, C. Sanchez-Hanke, Y. Wu, F. de Groot, L. Allard, and E. Lara-Curzio, IEEE Trans. Magn. **48**, 1710 (2012).
[12] N. Ji, X. Liu, and J.-P. Wang, New J. Phys. **12**, 063032 (2010).
[13] N. Ji, L. F. Allard, E. Lara-Curzio, and J.-P. Wang, Appl. Phys. Lett. **98**, 092506 (2011).
[14] M. van Schilfgaarde, T. Kotani, and S. Faleev, Phys. Rev. Lett. **96**, 226402 (2006).
[15] T. Kotani, M. van Schilfgaarde, and S. V. Faleev, Phys. Rev. B **76**, 165106 (2007).
[16] E. Y. Jiang, H. Y. Wang, and Z. W. Ma, J. Appl. Phys. **85**, 4488 (1999).
[17] H. Y. Wang, E. Y. Jiang, H. L. Bai, Y. Wang, P. Wu, and Y. G. Liu, J. Phys. D: Appl. Phys. **30**, 2932 (1997).
[18] H. Takahashi, M. Igarashi, A. Kaneko, H. Miyajima, and Y. Sugita, IEEE Trans. Magn. **35**, 2982 (1999).
[19] S. Uchida, T. Kawakatsu, A. Sekine, and T. Ukai, J. Magn. Magn. Mater. **310**, 1796 (2007).
[20] M. Methfessel, M. van Schilfgaarde, and R. A. Casali, in *Lecture Notes in Physics*, edited by H. Dreysse (Springer-Verlag, Berlin, 2000), Vol. 535.
[21] O. K. Andersen, Phys. Rev. B **12**, 3060 (1975).
[22] T. Kotani and M. van Schilfgaarde, Phys. Rev. B **81**, 125117 (2010).
[23] A. Liechtenstein, M. Katsnelson, V. Antropov, and V. Gubanov, J. Magn. Magn. Mater. **67**, 65 (1987).
[24] M. van Schilfgaarde and V. P. Antropov, J. Appl. Phys. **85**, 4827 (1999).
[25] V. Antropov, J. Magn. Magn. Mater. **262**, L192 (2003).
[26] T. Kotani and M. van Schilfgaarde, J. Phys.: Condens. Matter **20**, 295214 (2008).
[27] P. W. Anderson, in *Theory of Magnetic Exchange Interactions: Exchange in Insulators and Semiconductors*, edited by F. Seitz and D. Turnbull, Vol. 14 of Solid State Physics (Academic Press, New York, 1963), pp. 99–214.
[28] J. Rusz, I. Turek, and M. Diviš, Phys. Rev. B **71**, 174408 (2005).
[29] I. Turek, V. Drchal, J. Kudrnovský, M. Sob, and P. Weinberger, *Electronic Structure of Disordered Alloys, Surfaces and Interfaces* (Kluwer Academic Publishers, Boston, 1997).
[30] J. Kudrnovský and V. Drchal, Phys. Rev. B **41**, 7515 (1990).
[31] A. I. Lichtenstein, V. Antropov, and V. Gubanov, Phys. Met. Metal. **64**, 35 (1987).
[32] U. von Barth and L. Hedin, J. Phys. C **5**, 1629 (1972).
[33] J. P. Perdew, K. Burke, and M. Ernzerhof, Phys. Rev. Lett. **77**, 3865 (1996).
[34] H. Sawada, A. Nogami, T. Matsumiya, and T. Oguchi, Phys. Rev. B **50**, 10004 (1994).
[35] S. Matar, Z. Phys. B Condens. Matter **87**, 91 (1992).
[36] E. Kita, K. Shibata, H. Yanagihara, Y. Sasaki, and M. Kishimoto, J. Magn. Magn. Mater. **310**, 2411 (2007).
[37] N. Ji, M. S. Osofsky, V. Lauter, L. F. Allard, X. Li, K. L. Jensen, H. Ambaye, E. Lara-Curzio, and J.-P. Wang, Phys. Rev. B **84**, 245310 (2011).
[38] J. C. Slonczewski, Phys. Rev. **110**, 1341 (1958).
[39] R. L. Streever, Phys. Rev. B **19**, 2704 (1979).
[40] T. Burkert, O. Eriksson, P. James, S. I. Simak, B. Johansson, and L. Nordström, Phys. Rev. B **69**, 104426 (2004).
[41] A. N. Chantis, M. van Schilfgaarde, and T. Kotani, Phys. Rev. B **76**, 165126 (2007).